ADVANCED ELECTRONIC MATERIALS
www.advelectronicmat.de

Lateral Growth of MoS_2 2D Material Semiconductors Over an Insulator Via Electrodeposition

Nema M. Abdelazim, Yasir J. Noori, Shibin Thomas, Victoria K. Greenacre, Yisong Han, Danielle E. Smith, Giacomo Piana, Nikolay Zhelev, Andrew L. Hector, Richard Beanland, Gillian Reid, Philip N. Bartlett, and Cornelis H. de Groot**

Developing novel techniques for depositing transition metal dichalcogenides is crucial for the industrial adoption of 2D materials in optoelectronics. In this work, the lateral growth of molybdenum disulfide (MoS_2) over an insulating surface is demonstrated using electrochemical deposition. By fabricating a new type of microelectrodes, MoS_2 2D films grown from TiN electrodes across opposite sides are connected over an insulating substrate, hence, forming a lateral device structure through only one lithography and deposition step. Using a variety of characterization techniques, the growth rate of MoS_2 is shown to be highly anisotropic with lateral to vertical growth ratios exceeding 20-fold. Electronic and photo-response measurements on the device structures demonstrate that the electrodeposited MoS_2 layers behave like semiconductors, confirming their potential for photodetection applications. This lateral growth technique paves the way toward room temperature, scalable, and site-selective production of various transition metal dichalcogenides and their lateral heterostructures for 2D materials-based fabricated devices.

1. Introduction

Molybdenum disulfide is a 2D transition metal dichalcogenide (TMDC) semiconductor material that has been used as a building block in demonstrations of high on/off ratio transistors, ultrasensitive photodetectors, and sensors.[1–4] Some of these demonstrations were implemented for wearable applications by exploiting the material's exceptional robustness and flexibility.[5,6] However, there remain major obstacles that hinder the industrial adoption of MoS_2 and other 2D TMDC materials. The most challenging obstacle has been finding an industrially compatible method that enables the production of these materials on a mass scale. We have recently demonstrated that electrodeposition is a potentially viable method for solving this challenge.[7,8] Electrodeposition offers important advantages in 2D material production over other methods such as chemical vapor deposition (CVD),[9,10] sputtering,[11] or atomic layer deposition (ALD).[12] Electrodeposition is not a line-of-sight deposition method as material growth occurs at electrical contacts and is controlled by electrical potential or current.[13] It can hence be utilized to deposit materials over 3D surfaces including patterned nanostructures of high aspect ratios.[14–17] In addition, electrodeposition is usually performed at room temperature, avoiding harsh environments such as plasma or extremely high temperatures, which can damage pre-existing materials on the substrate, such as graphene electrodes.[7]

However, there is an important limitation with electrodeposition that needs to be overcome. This method requires an electrically conductive surface from which materials are traditionally grown vertically.[18] Depositing a semiconductor material on a conductor provides a low resistance current path in planar (opto-) electronic devices such as transistors and photodetectors, thus limiting the use of electrodeposition traditionally to certain vertical device structures or metal interconnects (through the dual damascene process).[19] Prior to the work described herein, this limitation has been a drawback, specifically for developing 2D material based devices where planar structures that exploit the unique 2D properties of the material are the "natural" route forward.[20–23]

Creating innovative techniques to electrodeposit planar 2D materials over non-conducting surfaces would solve this limitation and open new routes where the insulator base can be utilized, such as in transistor gating. In the early 1990s, Nishizawa et al. described the electrochemical growth of poly(pyrrole)

Dr. N. M. Abdelazim, Dr. Y. J. Noori, Dr. G. Piana, Prof. C. H. de Groot
Electronics and Computer Science
University of Southampton
Southampton SO17 1BJ, UK
E-mail: y.j.noori@southampton.ac.uk; chdg@ecs.soton.ac.uk
Dr. S. Thomas, Dr. V. K. Greenacre, Dr. D. E. Smith, N. Zhelev, Prof. A. L. Hector, Prof. G. Reid, Prof P. N. Bartlett
School of Chemistry, University of Southampton
Southampton SO17 1BJ, UK
Dr. Y. Han, Prof. R. Beanland
Department of Physics
University of Warwick
Coventry CV4 7AL, UK
The ORCID identification number(s) for the author(s) of this article can be found under https://doi.org/10.1002/aelm.202100419.

DOI: 10.1002/aelm.202100419

from an electrode out over the surface of an insulator, controlled by modification of the insulator surface.[24–26] More recently, Kobayashi et al. has showed that the lateral growth rate of Au from an Au electrode film can be increased via the surface treatment of SiO_2.[27] However, these are relatively rare examples. Furthermore, these demonstrations required surface treatment, and were limited to certain materials which severally restrict the scope of device applications that this technique can be employed for.

In this paper, we exploited the lateral growth technique for producing 2D TMDC semiconductors and their devices. We demonstrated strong anisotropy in the lateral growth rate of ultra-thin binary MoS_2 compounds via the electrodeposition over insulating substrates. By fabricating a new microelectrode structure that has its top coated with an insulator but its side edges exposed, we were able to restrict the growth of MoS_2 to favor the lateral growth direction for several micrometers, starting from these thin edges. The anisotropic growth along the lateral direction is demonstrated by transmission electron microscopy to be particularly attractive for 2D materials due to their unique planar layered structures. Using various material characterization techniques, we have shown that the lateral growth rate of MoS_2 across the insulator is 20-fold larger than its vertical growth rate. Furthermore, we have discovered that the lateral growth rate is linear, which allowed us to controllably connect two MoS_2 films grown from electrodes positioned on opposite sides across an insulator. This approach enabled us to realize a MoS_2 based device structure via a single lithography step. Finally, we demonstrated that our laterally grown MoS_2 films are semiconductors by developing an array of photodetector devices.

2. Fabrication and Electrodeposition

2.1. Lateral Growth Electrodes Fabrication

An illustration of the concept of our work on the lateral electrodeposition of MoS_2 is shown in **Figure 1**a. The TiN electrodes were fabricated on a SiO_2/Si substrate using a single photolithographic step as shown in Figure S1, Supporting Information. First, a negative photoresist was spin-coated on a wafer and then UV exposed using a photolithographic mask to form the desired pattern. TiN and SiO_2 were then consecutively sputtered on the wafer and a lift-off was performed to form the lateral growth electrodes. The thickness of the sputtered TiN layer is ≈100 nm. The double layer lift-off was executed to minimize the number of fabrication steps and eliminate the possibility of misalignment between the two sputtered layers that could result from performing multiple lithographic steps. A microscope image of the fabricated electrodes is shown in Figure 1b. The wafer was then diced into smaller chips prior to MoS_2 electrodeposition. An illustration of the chip layout is shown in Figure S2, Supporting Information. After MoS_2 deposition, each chip is cleaved into two halves through the cleave zone to disconnect the global electrode and create individual devices.

While all of the electrodes fabricated in this work were based on TiN, this fabrication technique should in principle be applicable to electrodes based on other materials, such as Au. However, challenges may arise due to alloying between the electrode material with the deposit, especially during annealing at high temperatures. The advantage of using TiN is that it does not alloy easily due to its Ti—N covalent bonds in the lattice.

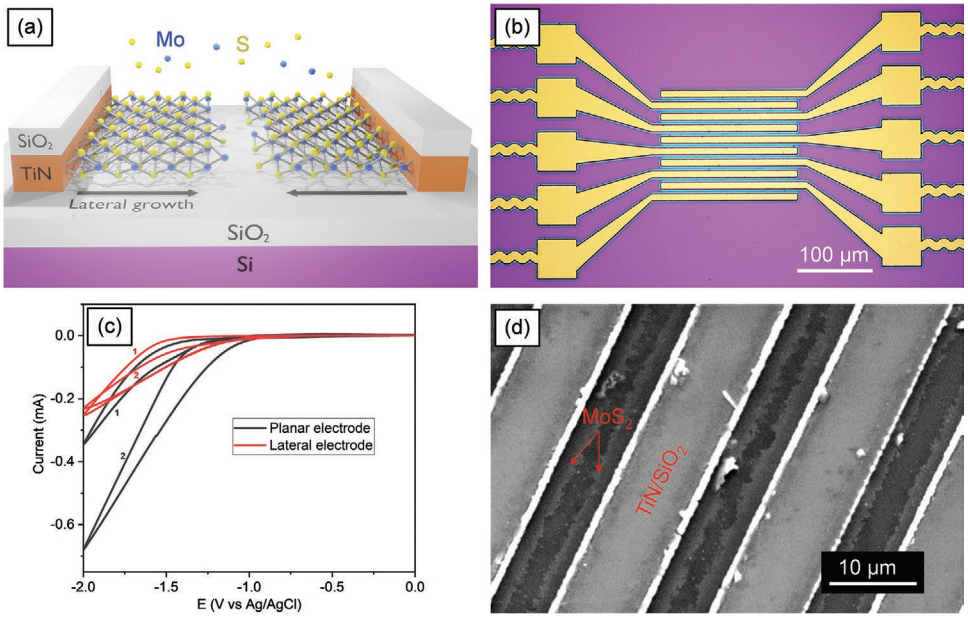

Figure 1. a) An illustration of the concept of this work showing TiN electrodes that are top covered with a SiO_2 insulator with a TMDC MoS_2 film growing laterally on the SiO_2/Si substrate. b) A microscope image of the fabricated electrode structure showing ten adjacent electrodes each connected to a pad for electrical contact. The light blue color surrounding the edges of the electrodes is laterally grown MoS_2. c) Cyclic voltammetry electrodeposition scans comparison between a large-area planar TiN electrode (diameter 4 mm) and one of the TiN lateral growth electrodes. d) An SEM image showing four TiN electrodes and three micro-gaps that are partially filled with laterally grown MoS_2 films via electrodeposition.

2.2. Electrodeposition of MoS_2

The electrodeposition experiments were performed in CH_2Cl_2 solvent using $[N^nBu_4]_2[MoS_4]$, which was synthesized in-house to function as a single source precursor, providing both the Mo and S.[7,8] In contrast to $[NH_4]_2[MoS_4]$, which has been used in aqueous solvents, $[N^nBu_4]_2[MoS_4]$ has excellent solubility in CH_2Cl_2. The electrodeposition solution also included $[N^nBu_4]Cl$ as the supporting electrolyte and trimethylammonium chloride $[NHMe_3]Cl$ as the proton source, which is necessary to remove the excess S during deposition of MoS_2 from $[MoS_4]^{2-}$.[8] The electrodeposition experiments were all performed within a glovebox equipped with a dry nitrogen circulation system to minimize moisture and ensure that oxygen levels were maintained below 10 ppm. The depositions were performed using a three electrode electrochemical cell with a Pt gauze as counter electrode and a Ag/AgCl (0.1 M $[N^nBu_4]Cl$ in CH_2Cl_2) reference electrode.

Cyclic voltammetry (CV) scans were performed to study the electrochemical behavior of the electrolyte with the lateral growth electrodes. Figure 1c shows the comparison of CVs recorded on a TiN fabricated electrode and a 4 mm diameter planar TiN electrode. The CVs are obtained by sweeping the voltage from 0 to −2.0 V in the cathodic scan and then −2.0 to 0 V in the anodic scan. On the first cycle, there is evidence of a nucleation process in both cases with the current being increased on the return and on subsequent scans. This occurs because the deposited MoS_2 functions as a catalyst for the reduction of the $NHMe_3^+$ which results in hydrogen evolution. We recently reported a detailed investigation on the electrochemical processes during the CV of the same electrolyte system employing electrochemical quartz crystal microbalance (EQCM) measurements.[8] The CVs displayed in Figure 1c clearly show evidence of the cathodic reduction of $[MoS_4]^{2-}$ ions to MoS_2. It is clear that the CV recorded from the lateral TiN electrodes is comparable, in terms of electrochemical processes at the interface, to the CV measured on the planar TiN electrode, indicating that the electro-reduction mechanism of the $[MoS_4]^{2-}$ ions remains the same irrespective of the type of TiN electrode used.

The lateral growth of MoS_2 was achieved through potentiostatic electrodeposition by applying −1.0 V and varying the deposition time to achieve the desired lateral growth length. The electrochemical reactions at the working and counter electrodes respectively, are as follows

$$MoS_4^{2-} + 2e^- + 4H^+ \rightarrow MoS_2 + 2H_2S \quad (1)$$

$$MoS_4^{2-} \rightarrow MoS_3 + \frac{1}{8}S_8 + 2e^- \quad (2)$$

Following electrodeposition, the sample was rinsed with CH_2Cl_2 and left to dry inside the glove box. The as-deposited MoS_2 film is amorphous, as X-ray diffraction on thicker films indicate, although with some short-range ordering present as evidenced by the preferential lateral growth.[8,28–30] An annealing step was performed to crystallize the film. The sample was annealed using a tube furnace that was set initially to 100 °C for 10 min and then 500 °C for 2 h at 0.1 mbar. Annealing the films was performed within a sulfur rich environment made by placing 0.1 g of sulfur powder together with the sample inside the quartz tube within the tube furnace. To prevent distillation of volatile sulfur from the film and cause it to become understoichiometric, a sulfur rich environment was used. Thermal annealing was found to substantially improve the crystallinity of the film as evidenced by Raman Spectroscopy.[7,8] It also removed excess sulfur from the film.

3. Results and Discussions

3.1. Microscopy

On applying an electrodeposition potential to the electrode array, the material starts to grow from the side edges of each electrode. Throughout this work, the deposition time was chosen to be either 20, 45, or 90 min. Figure 1b shows an optical microscope image of patterned electrodes with laterally grown MoS_2 films depicted by the light blue borders surrounding the yellow electrodes. Figure 1d shows a scanning electron microscope (SEM) image of a laterally grown MoS_2 film from the edges of TiN electrodes. The contrast difference between the laterally grown MoS_2 films and the SiO_2 covered substrate underneath can be clearly observed. Figure S3a–c, Supporting Information, shows SEM images of laterally grown films deposited for 20, 45, and 90 min. By observing the electrodeposition length with time, we were able to allow the laterally grown films from adjacent electrodes to contact in the middle region by electrodepositing for 90 min.

Figure 2a–d shows atomic force microscopy (AFM) images performed across the growth regions between two adjacent electrodes from a pristine substrate and ones with laterally grown MoS_2 films. Typical line profiles for each film are shown in Figure 2e. After 20 minutes of deposition (Figure 2b), the AFM images show clear initial growth of the film laterally from both sides of the electrodes. Upon increasing the deposition time to 45 min (Figure 2c), the film near to the electrodes were found to be smoother and continuous. However, it is clear from the figure that 45 min is not sufficient to allow the films grown from opposite sides to contact each other. Figure 2d shows an AFM image of a film grown for 90 minutes. In the latter deposition, the two films were found to meet in the center between the electrodes above the SiO_2 substrate, causing one film to grow over the other, resulting in a small peak in the AFM profile in the middle region.

3.2. Films Thickness and Length

Figure 2f shows that the lateral growth length scales linearly with the deposition time. An average growth rate of 33 ± 6 nm min^{-1} was extracted. The error bars represent the maximum and minimum observed growth lengths. The lateral growth length measurements were recorded on the films that were grown out of the uppermost electrode from the ten-electrode array shown in Figure 1b. This was chosen to prevent

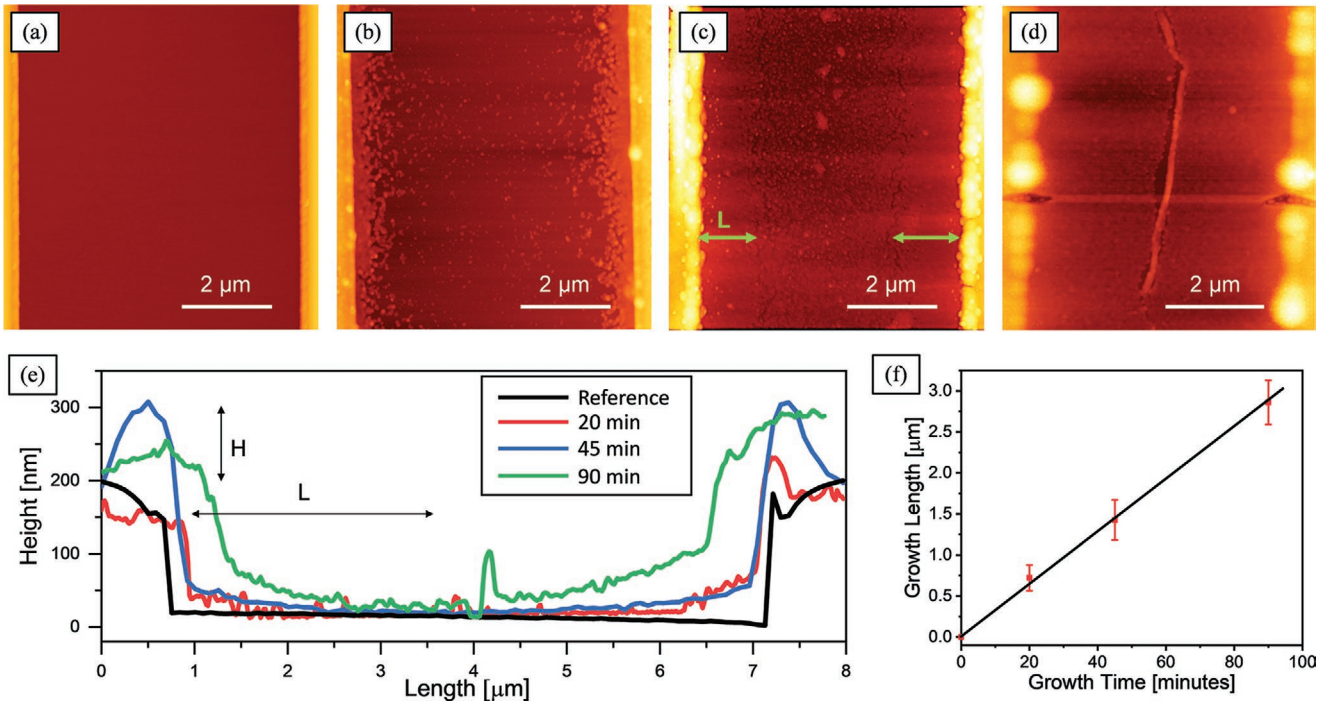

Figure 2. AFM images of a) reference sample and b–d) laterally grown films deposited for b) 20 min, c) 45 min, and d) 90 min after annealing. e) Topography line profiles collected from images (a–d). The figure shows indications of the vertical growth (H) and lateral growth (L) that were considered for analysis in this work. f) A linear fit of the growth length versus time obtained from the three samples.

connecting layers from introducing uncertainties in the length measurements. Each experiment with a particular deposition time was replicated to ensure experimental reproducibility. The average lengths and uncertainties were calculated over ten AFM measurements from every sample. To quantify the thickness and length of the grown films, topography profiles were acquired from five lines across AFM images corresponding to films grown for 20, 45, and 90 min as shown in Figure S4a, Supporting Information. The average values of the vertical (height) and lateral growths (length) were extracted for each film. The average heights above the edge of the electrodes (H_{av}), lengths (L_{av}), and their corresponding maximum (H_{max} and L_{max}) values were recorded in Table S1, Supporting Information. Figure S4b, Supporting Information, shows the L_{av} and H_{av} measurements taken from five different lines across the 20, 45, and 90 min grown films. By comparing the values of H versus W, we found that the lateral growth rate is ≈20 times larger than the vertical growth. In these experiments, the electrodes thickness was fixed to 100 nm. We think that using thinner electrodes will increase the growth anisotropy, due to surface effects, compared to thicker ones but will not suppress the vertical growth rate completely.

As the electrodeposition time is increased, the vertical growth of the material becomes more prominent, especially near the electrodes where the film growth starts. We observed that the vertically grown materials can be thick enough to rise above the fabricated TiN/SiO_2 electrodes and start to grow laterally over the top insulated electrodes. However, it is clear that the vertical growth rate of MoS_2 is much slower than the lateral growth rate.

3.3. Raman Spectroscopy

Raman spectroscopy is a commonly used technique in characterizing different physical properties of TMDC 2D materials. We used this method to confirm the presence of the MoS_2 films and qualitatively study their degree of crystallinity and lateral growth length. All measurements were performed using a 532 nm excitation laser at room temperature. A 50× objective lens was used to focus the excitation laser to an ≈1 μm spot diameter and simultaneously collect the emitted light. **Figure 3**a shows three Raman spectra collected from different locations around the electrodes using a sample with a MoS_2 film grown for 45 min. Point A is in the center between the two electrodes, point B is above one of the electrodes, and point C is on a blank SiO_2/Si region of the substrate, away from the electrodes. These locations are shown in the inset of the figure. The MoS_2 Raman signature corresponding to the E^1_{2g} and the A_{1g} peaks was only found at point A, demonstrating that there is no deposition at the center above the top insulated TiN electrodes, nor on the SiO_2 substrate away from the electrodes. The central positions of the E^1_{2g} and A_{1g} peaks are 382.5 and 405.6 cm^{-1}, respectively. Energy dispersive X-ray (EDX) spectroscopy spectra are shown in Figure S5, Supporting Informtation. Due to the large overlap between the Mo and S electron emission lines (≈2.3 keV), EDX is not a reliable technique to measure the elemental composition. It was therefore only used to identify the nature of the materials at different regions of the sample, utilizing the much higher image resolution offered by the SEM compared to optical techniques. The EDX spectra show Mo and S signatures solely above the laterally grown films, confirming the conclusion of

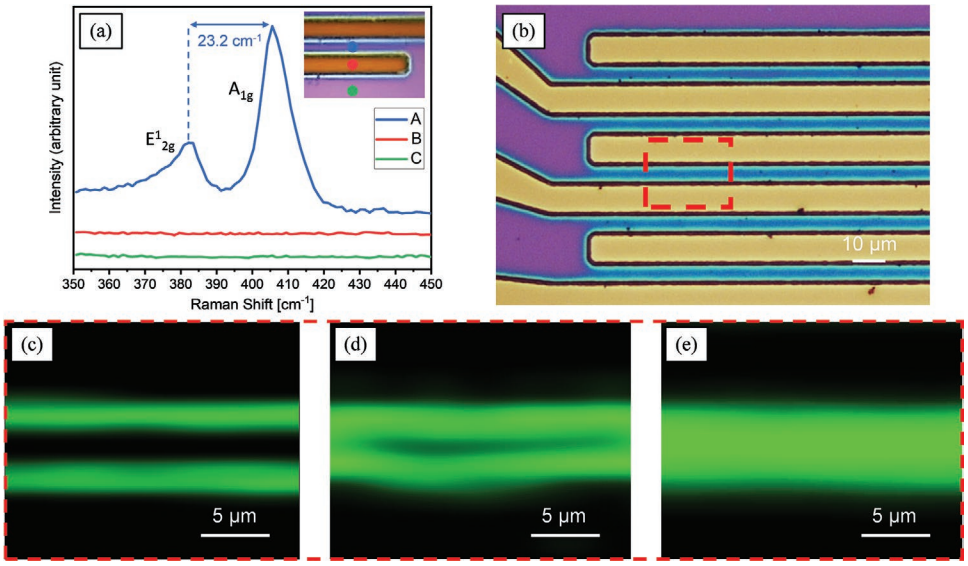

Figure 3. a) A stack of Raman spectra showing that the MoS_2 signal is solely observed from the laterally grown films with no Raman signatures from areas away from the electrodes or at the center above them. b) An optical microscope image of a series of fabricated TiN micro-electrodes with laterally grown MoS_2 films (90 min) that are showing as light blue borders surrounding the electrodes. c–e) Raman maps of areas corresponding to that of the red box in (b) between adjacent electrodes for films grown for 20, 45, and 90 min, respectively. The maps show a clear increase in the lateral length of the MoS_2 films with increasing the deposition time.

the Raman images. In previous works, we characterized the material composition of MoS_2 films electrodeposited via similar electrochemical environments using wavelength dispersive X-ray spectroscopy (WDX) and X-ray photoelectron spectroscopy (XPS).[7,8] These results have shown that the Mo:S ratio is ≈1:2.

Raman mappings were performed on selected areas as exemplified in Figure 3b, of 20, 45, and 90 min grown films using the A_{1g} peak signal intensity and a step size of ≈1 μm, see Figure 3c–e. The maps show the evolution of the lateral growth as the electrodeposition time is increased, causing the films grown from opposite sides to slowly merge after ≈90 min deposition. However, the fact that the laser spot is ≈1 μm means that the exact distribution of the material cannot be precisely defined through this method. The combined results of AFM, SEM, and Raman mapping clearly confirm the lateral growth of MoS_2 across the SiO_2 insulator after starting from the thin edges of the TiN electrodes.

3.4. Transmission Electron Microscopy

Figure 4a shows a high-resolution cross section SEM image of a laterally grown film. The cross-section was taken after performing a lamella process using a focused ion beam (FIB). The image shows the MoS_2 thin film grown over the SiO_2/Si substrate and covered by Pt and C protection layers that were deposited during the lamella process. It can be seen that the film gets thinner further away from the electrode toward the left of the image. Annular dark field (ADF) TEM imaging was then used to reveal the nanocrystalline structure of MoS_2 layers. The ADF mode allows distinguishing MoS_2 from its surrounding SiO_2 and Pt. Figure 4b shows a laterally grown film which was deposited for 90 min. We noticed that the stacked layers are generally aligned in the lateral growth direction perpendicular to the plane of the substrate. In a film grown for 45 min, presented in Figure 4c,d, TEM imaging reveals that the film is much thinner and where the layers are more ordered. This suggests that the amount of ordering correlates inversely with the thickness of the films. The layer-to-layer distance of the ordered stack shown in Figure 4c was measured to be 0.7 ± 0.1 nm, which is in agreement with literature values of MoS_2 layers spacing measurements.[31] Conventional X-ray diffraction is not suitable to test the crystallinity of these laterally grown films due to their small area and thickness. However, X-ray diffraction performed on large area and thick deposition attempts performed in similar environments showed the appearance of a crystallisation peak corresponding to (002) plane of 2H-MoS_2 following film annealing.[8] The TEM results of the laterally grown films presented here show that the films are polycrystalline with layer sizes in the order of tens of nanometers.

3.5. Photoresponsivity of Laterally Grown MoS_2 Devices

Electrical characterization of the laterally grown films was performed by connecting adjacent lateral growth electrodes to a semiconductor device analyzer. **Figure 5**a shows current-voltage sweeps taken from films that were grown for 20, 45, and 90 min. The displayed curves were taken from different films that were grown in multiple repeat experiments. The electrical connection between the electrodes for the 20 min sample is open, while that for the 45 min sample, has resistance exceeding 500 MΩ. The electrical resistance was measured to be significantly lower for the 90 min sample after the laterally grown films from both sides had connected in the middle. The inset of the figure shows ohmic behavior with a resistance of ≈1 MΩ. Using the length

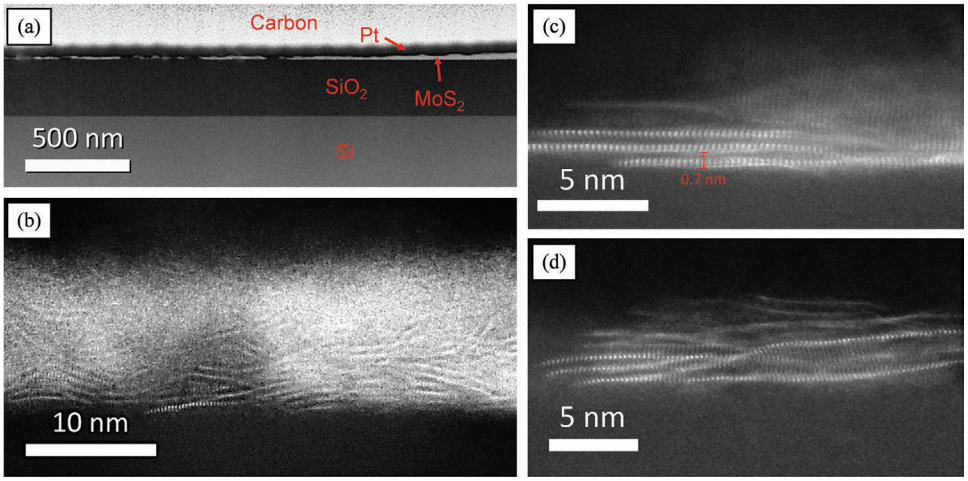

Figure 4. a) A high-resolution SEM image of a cross-section of a region between two electrodes with a laterally grown MoS_2 film. The film was coated with Pt and C protective layers. b) A magnification of the MoS_2 film shown in (a) taken via TEM that clearly shows the layered nature of the film growing preferentially in the horizontal direction along the surface of the wafer. The film was taken from a sample that was grown for 90 min. c,d) TEM images of a few layers of MoS_2 taken at a thin region from a film that was grown for 45 min.

and width of the channel and the estimated average thickness of the films (≈60 nm), we extract the room temperature resistivity of the 90 min grown films as 115 Ω.cm. This resistivity is in the range of earlier reported MoS_2 films.[32]

The photoresponsivity of the MoS_2 films was tested at room temperature in air, using a 532 nm laser source. The aim of this experiment was to test the film's semiconductor optical absorption and induced current. The tests were performed by applying

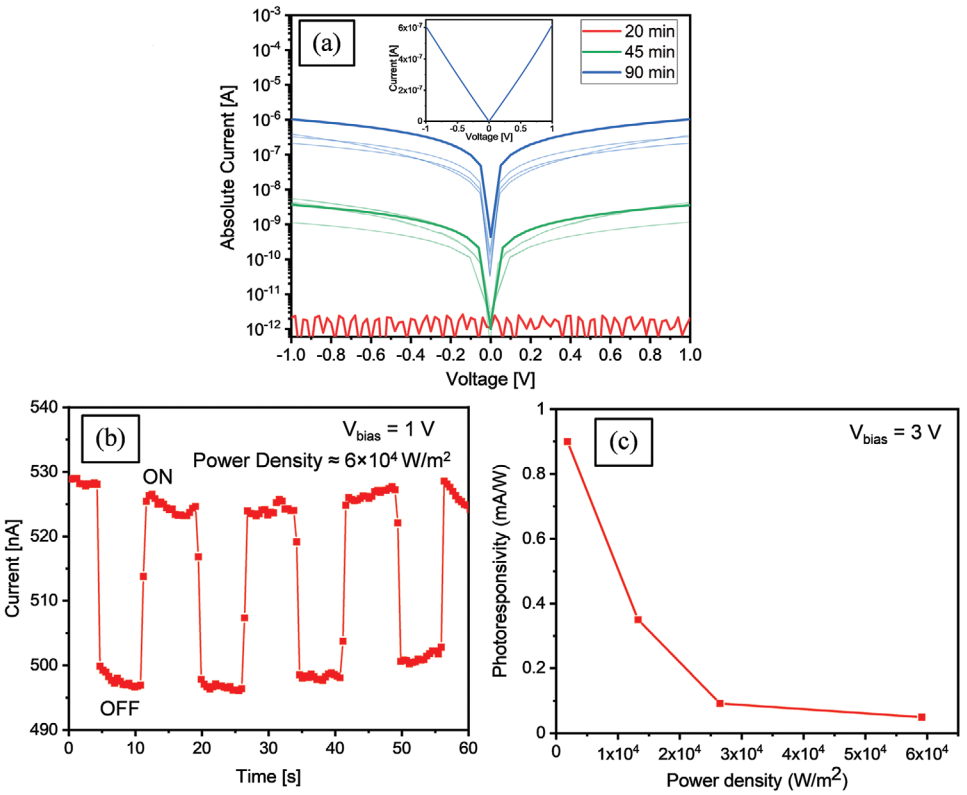

Figure 5. a) Multiple Current–Voltage sweeps from MoS_2 devices grown multiple times for 20, 45, and 90 min showing an open circuit after 20 min film growth and a great increase in current from 45 min growth to 90 min. The inset is a replot of the 90m sample on a linear scale. b) Photo-illumination cycles of a sample showing the switching induced photocurrent with a switching laser source. c) The change in photoresponsivity as the power density of the excitation laser is changed.

a bias voltage on two adjacent electrodes and the current was measured through the device in the dark and under laser illumination. The laser light was coupled to the chip through a fiber and a long distance 20× objective lens, reducing the spot size to a circular spot with a diameter of roughly 100 µm. Figure 5b presents the photocurrent induced in the material due to a pulsing laser. The applied bias, $V_{bias} = 1$ V and the laser power density was calculated to be $\approx 6 \times 10^4$ Wm^{-2}. The photoresponsivity of the film was calculated using Equation (3) below:

$$\text{Photoresponsivity} = \frac{I_{ph}}{P_{laser}} \tag{3}$$

where I_{ph} is the photoinduced current. I_{ph} can be calculated by subtracting the device current under illumination from the dark current $I_{ph} = I_{light} - I_{dark}$ and P_{laser} is the incident laser power. Several measurements were made on different chips containing devices of films grown for 90 min. The maximum photoresponsivity recorded was 0.9 mA W^{-1}. We then performed photoresponsivity measurements at varying laser power densities as shown in Figure 5c.

It was found that the photoresponsivity reduces at higher laser power density, indicating carrier saturation in the material. Whilst this photoresponsivity is higher than our previously reported values from the electrodeposition method,[7] it is still lower than previously reported from MoS_2 films made via CVD and mechanical exfoliation.[33,34] This is expected to be due to the lower material crystallinity produced from electrodeposition in comparison to the other aforementioned methods. Our future work will include using a similar structure to develop phototransistor devices using the bottom SiO_2 as a back-gate dielectric.[2,9]

4. Conclusion

We have demonstrated the lateral electrodeposition of transition metal dichalcogenide (TMDC) films over an insulating substrate for optical and electrical measurements. The MoS_2 is deposited directly onto patterned electrodes using a non-aqueous electrodeposition method. The nature of the deposition is such that the material growth occurs from the side edges of 100 nm thick TiN electrodes. The electrodeposition duration determines the extent of the material's lateral growth. By fabricating adjacent electrodes and exploiting the preference of the material to grow laterally, we have shown the ability to grow films from opposite sides toward each other until they connect in the middle. The deposited films were characterized using a variety of techniques including AFM, Raman, SEM, EDX, and TEM. The lateral growth length was found to increase linearly with the deposition time with an average rate of $\approx 33 \pm 6$ nm min^{-1}. This is ≈20 folds faster than the material's vertical growth. Electrical and photoresponsivity measurements of the MoS_2 films showed that the material is semiconducting. Our work provides an innovative, efficient, and scalable method for the lateral growth of 2D materials and promotes their applications in next-generation electronic and optoelectronic devices. This paves the way toward future possibilities such as electrodepositing different TMDCs to form lateral heterostructures of 2D materials, creating novel p–n–p junction in a single electrodeposition experiment.[35,36]

Supporting Information

Supporting Information is available from the Wiley Online Library or from the author.

Acknowledgements

N.M.A., Y.J.N., and S.T. contributed equally to this work. The research work reported in this article was financially supported by the Engineering and Physical Sciences Research Council (EPSRC) through the research grant EP/P025137/1 (2D layered transition metal dichalcogenide semiconductors via non-aqueous electrodeposition) and the programme grant EP/N035437/1 (ADEPT – Advanced Devices by ElectroPlaTing).

Conflict of Interest

The authors declare no conflict of interest.

Data Availability Statement

All data supporting this study are openly available from the University of Southampton repository at DOI: https://doi.org/10.5258/SOTON/D1856. Additional data from this study are available from the corresponding author upon reasonable request.

Keywords

electrodeposition, 2D-materials, MoS_2, photodetectors, transition metal dichalcogenides

Received: April 23, 2021
Revised: June 3, 2021
Published online:

[1] X.-F. Wang, H. Tian, Y. Liu, S. Shen, Z. Yan, N. Deng, Y. Yang, T.-L. Ren, *ACS Nano* **2019**, *13*, 2205.
[2] Z. Yin, H. Li, H. Li, L. Jiang, Y. Shi, Y. Sun, G. Lu, Q. Zhang, X. Chen, H. Zhang, *ACS Nano* **2012**, *6*, 74.
[3] H. S. Nalwa, *RSC Adv.* **2020**, *10*, 30529.
[4] R. Kumar, W. Zheng, X. Liu, J. Zhang, M. Kumar, *Adv. Mater. Technol.* **2020**, *5*, 1901062.
[5] S. Bertolazzi, J. Brivio, A. Kis, *ACS Nano* **2011**, *5*, 9703.
[6] N. Li, Q. Wang, C. Shen, Z. Wei, H. Yu, J. Zhao, X. Lu, G. Wang, C. He, L. Xie, J. Zhu, L. Du, R. Yang, D. Shi, G. Zhang, *Nat. Electron.* **2020**, *3*, 711.
[7] Y. J. Noori, S. Thomas, S. Ramadan, D. E. Smith, V. K. Greenacre, N. Abdelazim, Y. Han, R. Beanland, A. L. Hector, N. Klein, G. Reid, P. N. Bartlett, C. H. Kees de Groot, *ACS Appl. Mater. Interfaces* **2020**, *12*, 49786.
[8] S. Thomas, D. E. Smith, V. K. Greenacre, Y. J. Noori, A. L. Hector, C. H. (Kees) de Groot, G. Reid, P. N. Bartlett, *J. Electrochem. Soc.* **2020**, *167*, 106511.
[9] W. Zhang, J.-K. Huang, C.-H. Chen, Y.-H. Chang, Y.-J. Cheng, L.-J. Li, *Adv. Mater.* **2013**, *25*, 3456.

[10] J. Chen, W. Tang, B. Tian, B. Liu, X. Zhao, Y. Liu, T. Ren, W. Liu, D. Geng, H. Y. Jeong, H. S. Shin, W. Zhou, K. P. Loh, *Adv. Sci.* **2016**, *3*, 1500033.
[11] J. Tao, J. Chai, X. Lu, L. M. Wong, T. I. Wong, J. Pan, Q. Xiong, D. Chi, S. Wang, *Nanoscale* **2015**, *7*, 2497.
[12] X. Tang, N. Reckinger, O. Poncelet, P. Louette, F. Ureña, H. Idrissi, S. Turner, D. Cabosart, J.-F. Colomer, J.-P. Raskin, B. Hackens, L. A. Francis, *Sci. Rep.* **2015**, *5*, 13523.
[13] A. A. Ojo, I. M. Dharmadasa, *Coatings* **2018**, *8*, 262.
[14] N. J. Gerein, J. A. Haber, *J. Phys. Chem. B* **2005**, *109*, 17372.
[15] H.-F. Wang, C. Tang, Q. Zhang, *Nano Today* **2019**, *25*, 27.
[16] R. Huang, G. P. Kissling, R. Kashtiban, Y. J. Noori, K. Cicvarić, W. Zhang, A. L. Hector, R. Beanland, D. C. Smith, G. Reid, P. N. Bartlett, C. H. (Kees) de Groot, *Faraday Discuss.* **2019**, *213*, 339.
[17] P. N. Bartlett, S. L. Benjamin, C. H. (Kees) de Groot, A. L. Hector, R. Huang, A. Jolleys, G. P. Kissling, W. Levason, S. J. Pearce, G. Reid, Y. Wang, *Mater. Horizons* **2015**, *2*, 420.
[18] J. L. Hudson, T. T. Tsotsis, *Chem. Eng. Sci.* **1994**, *49*, 1493.
[19] P. C. Andricacos, C. Uzoh, J. O. Dukovic, J. Horkans, H. Deligianni, *IBM J. Res. Dev.* **1998**, *42*, 567.
[20] A. Sharma, R. Mahlouji, L. Wu, M. A. Verheijen, V. Vandalon, S. Balasubramanyam, J. P. Hofmann, W. M. M. (Erwin) Kessels, A. A. Bol, *Nanotechnology* **2020**, *31*, 255603.
[21] M. Chhowalla, D. Jena, H. Zhang, *Nat. Rev. Mater.* **2016**, *1*, 16052.
[22] F. Giannazzo, G. Greco, F. Roccaforte, S. S. Sonde, *Crystals* **2018**, *8*, 70.
[23] Y. Liu, N. O. Weiss, X. Duan, H.-C. Cheng, Y. Huang, X. Duan, *Nat. Rev. Mater.* **2016**, *1*, 16042.
[24] M. Nishizawa, M. Shibuya, T. Sawaguchi, T. Matsue, I. Uchida, *J. Phys. Chem.* **1991**, *95*, 9042.
[25] M. Nishizawa, Y. Miwa, T. Matsue, I. Uchida, *J. Electrochem. Soc.* **1993**, *140*, 1650.
[26] M. Nishizawa, T. Kamiya, H. Nozaki, H. Kaji, *Langmuir* **2007**, *23*, 8304.
[27] C. Kobayashi, M. Saito, T. Homma, *Electrochim. Acta* **2012**, *74*, 235.
[28] A. Albu-Yaron, *Electrochem. Solid-State Lett.* **1999**, *2*, 627.
[29] R. Chaabani, A. Lamouchi, B. Mari, R. Chtourou, *Mater. Res. Express* **2019**, *6*, 115902.
[30] A. Lamouchi, I. Ben Assaker, R. Chtourou, *J. Mater. Sci.* **2017**, *52*, 4635.
[31] J. Xiao, M. Long, X. Li, Q. Zhang, H. Xu, K. S. Chan, *J. Phys.: Condens. Matter* **2014**, *26*, 405302.
[32] G. Eda, H. Yamaguchi, D. Voiry, T. Fujita, M. Chen, M. Chhowalla, *Nano Lett.* **2011**, *11*, 5111.
[33] G. Wu, X. Wang, Y. Chen, Z. Wang, H. Shen, T. Lin, W. Hu, J. Wang, S. Zhang, X. Meng, J. Chu, *Nanotechnology* **2018**, *29*, 485204.
[34] N. Perea-López, Z. Lin, N. R. Pradhan, A. Iñiguez-Rábago, A. Laura Elías, A. McCreary, J. Lou, P. M. Ajayan, H. Terrones, L. Balicas, M. Terrones, *2D Mater.* **2014**, *1*, 11004.
[35] X. Duan, C. Wang, J. C. Shaw, R. Cheng, Y. Chen, H. Li, X. Wu, Y. Tang, Q. Zhang, A. Pan, J. Jiang, R. Yu, Y. Huang, X. Duan, *Nat. Nanotechnol.* **2014**, *9*, 1024.
[36] J. Wang, Z. Li, H. Chen, G. Deng, X. Niu, *Nano-Micro Lett.* **2019**, *11*, 48.